

Contents lists available at ScienceDirect

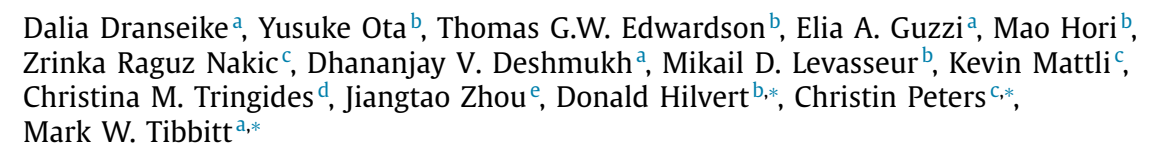
Acta Biomaterialia

journal homepage: www.elsevier.com/locate/actbio



Full length article

Designed modular protein hydrogels for biofabrication





- ^a Macromolecular Engineering Laboratory, ETH Zurich, Zurich, Switzerland
- ^b Organic Chemistry Laboratory, ETH Zurich, Zurich, Switzerland
- ^c Biosystems Technology, ZHAW, Wädenswil, Switzerland
- ^d Laboratory of Biosensors and Bioelectronics, ETH Zurich, Switzerland
- ^e Laboratory of Food and Soft Materials, ETH Zurich, Switzerland

ARTICLE INFO

Article history: Received 3 October 2023 Revised 1 February 2024 Accepted 13 February 2024 Available online 19 February 2024

Keywords: Biofabrication Protein design Biomaterials Protein hydrogels

ABSTRACT

Designing proteins that fold and assemble over different length scales provides a way to tailor the mechanical properties and biological performance of hydrogels. In this study, we designed modular proteins that self-assemble into fibrillar networks and, as a result, form hydrogel materials with novel properties. We incorporated distinct functionalities by connecting separate self-assembling (A block) and cell-binding (B block) domains into single macromolecules. The number of self-assembling domains affects the rigidity of the fibers and the final storage modulus G' of the materials. The mechanical properties of the hydrogels could be tuned over a broad range (G' = 0.1 - 10 kPa), making them suitable for the cultivation and differentiation of multiple cell types, including cortical neurons and human mesenchymal stem cells. Moreover, we confirmed the bioavailability of cell attachment domains in the hydrogels that can be further tailored for specific cell types or other biological applications. Finally, we demonstrate the versatility of the designed proteins for application in biofabrication as 3D scaffolds that support cell growth and guide their function.

Statement of significance

Designed proteins that enable the decoupling of biophysical and biochemical properties within the final material could enable modular biomaterial engineering. In this context, we present a designed modular protein platform that integrates self-assembling domains (A blocks) and cell-binding domains (B blocks) within a single biopolymer. The linking of assembly domains and cell-binding domains this way provided independent tuning of mechanical properties and inclusion of biofunctional domains. We demonstrate the use of this platform for biofabrication, including neural cell culture and 3D printing of scaffolds for mesenchymal stem cell culture and differentiation. Overall, this work highlights how informed design of biopolymer sequences can enable the modular design of protein-based hydrogels with independently tunable biophysical and biochemical properties.

© 2024 The Author(s). Published by Elsevier Ltd on behalf of Acta Materialia Inc. This is an open access article under the CC BY license (http://creativecommons.org/licenses/by/4.0/)

1. Introduction

Hydrogels are increasingly recognized for their use in facilitating cell growth for *ex vivo* tissue models [1], drug delivery [2,3],

E-mail addresses: donald.hilvert@org.chem.ethz.ch (D. Hilvert), petc@zhaw.ch (C. Peters), mtibbitt@ethz.ch (M.W. Tibbitt).

and biosensing [4]. The design of such hydrogel platforms is based on matching the biological and rheological requirements of the intended application [5,6]. Therefore, the tailoring of hydrogels demands a versatile engineering toolkit at different length scales, from macromolecule design to network architecture.

The diversity of natural proteins and peptides offers a broad spectrum of possibilities for the modular design of large molecular weight polymers that form hydrogels [7]. These hydrogels can be formed through site-specific covalent bonds [6,8], stimuli-

^{*} Corresponding authors.

responsive physical interactions [9], protein folding and hierarchical self-assembly [10–13]. Non-covalent networks are of particular interest as the inter- and intramolecular interactions can be formed at different length scales: from pi-pi stacking of peptide side chains [14], to folding into hairpin structures within the peptide sequence [15], to helix formation between different chains as crosslinks of flexible linker chains [16]. It creates a library of motifs for tailoring the mechanical behavior of the resulting hydrogel biomaterials for therapeutic applications [17].

Moreover, several types of hydrogel-forming peptide domains can be combined in a single macromolecule using recombinant technologies [18,19]. Further, the modular design of recombinant proteins allows the integration of self-assembly domains with bioactive moieties, e.g., including amino acid sequences for cell attachment or biomolecule-binding, within a single hydrogel forming polymer [20–22]. The ability to mix and match domains via modular design makes recombinant proteins an attractive material to create hydrogel platforms for tissue repair [23,24], biofabrication [19,25], and injectable drug delivery [26].

The formation of protein and peptide hydrogels often arises from the formation of fibrillar networks [27,28]. For example, the protein-based extracellular matrix (ECM), which is built and continuously remodeled by cells, is rich in fibrillar networks formed by collagen hierarchical assembly [29]. Another common motif in protein-based materials is beta-sheet stacking, which often results in amyloid fiber networks [30]. Amyloid-based hydrogels formed using amphiphilic peptides have been designed for neural regeneration [31] and hemostasis [32]. In addition, structural proteins, such as silk, assemble into composites with beta-sheet crystallites in a matrix to form mechanically robust biomaterials [33]. Based on this paradigm, designed proteins with silk-inspired, beta-sheet forming domains have been combined with elastin-like domains for bioprinting of cell-laden 3D structures [34]. Despite the utility of these hydrogels, it often challenging to design a platform with broad applicability, requiring a unique biopolymer to be engineered for each use case. In this context, recombinant proteins that assemble as tertiary amyloid structures and form fibrillar hydrogels could function as a modular biomaterial platform that can be engineered at different scales. Further, specific biological functionality and/or binding domains could be integrated in the protein backbone as separate modules exposed along or within the protein fibers [35].

In this work, we describe the bottom-up design of such a modular protein platform that forms fibrillar hydrogels (Fig. 1). The combination of distinct self-assembling (A block) and cell-binding (B block) domains linked together into single polymer chains was chosen to provide freedom for inclusion of desired functionalities. We produced two main variants using this design strategy: ABA and ABABA. Amphiphilic peptide sequences were used in the A block to allow self-assembly and formation of robust amyloid networks. The number of A and B domains controlled the selfassembly, fiber formation, and rheological properties of the formed hydrogels. The physical nature of the protein hydrogels combined with the accessibility of their cell-binding domains rendered them suitable for culture of different cell types and bioprinting. This modular protein platform provides a foundation that could be further tailored to the needs of specific biomedical applications via facile inclusion of additional functional domains.

2. Materials and methods

2.1. Preparation of plasmids

DNA sequences for structural proteins were codon optimized for expression in *E. coli*. DNA fragments encoding the structural protein genes were then produced by assembly polymerase chain re-

action (PCR) of shorter fragments. The QuikChange® (Agilent Technologies) method was used to introduce point mutations through PCR. All oligonucleotides used for cloning were purchased from Microsynth AG (Switzerland). PCR products were purified by 1.5% agarose gel, the bands cut out with reference to a DNA ladder (100 bp DNA Ladder, New England Biolabs) and isolated using a DNA gel extraction kit (Zymo Research).

The purified PCR products were cloned into the vector pET29b(+) through restriction site ligation. Ligation was performed using T4 DNA ligase (New England Biolabs) and the ligation reaction was used to transform chemically-competent *E. coli* strain XL1-Blue (Agilent) using a heat shock method adapted from Froger & Hall [36]. Successfully transformed clones were selected on lysogeny broth (LB) agar plates containing 100 µg mL⁻¹ kanamycin sulfate (PanReac AppliChem). Single colonies of transformants were grown in LB pre-cultures containing 50 µg mL⁻¹ kanamycin sulfate at 37°C overnight and harvested by centrifugation. Plasmids were isolated using a ZR Plasmid Miniprep-Classic kit (Zymo Research). Plasmid sequences were confirmed by Sanger DNA sequencing by Microsynth AG), using the T7 primer.

2.2. Protein expression, purification, and characterization

Expression of the novel proteins was performed in E. coli BL21(DE3). Flask cultivation was conducted in an orbital shaker using terrific broth (TB) medium (24 g L⁻¹ yeast extract, 12 g L^{-1} tryptone, 4 g L^{-1} glycerol, 0.072 M KH_2PO_4 and 0.017 M KH₂PO₄), supplemented with kanamycin (0.05 mg mL⁻¹). First, a 5 mL overnight preculture was incubated at 37°C and 180 rpm. Protein expression was performed either on a small or large scale. For small-scale protein expression, baffled flasks containing 400 mL media were inoculated with 4 mL preculture. Large-scale protein expression was performed in a 30 L batch using a 50 L roundbottom stirred fermenter (B. Braun Biotech International UD 50 Biostat). A 400 mL overnight flask culture was used for the inoculation of the TB medium, and 15 mL 20% PEG was supplemented as an antifoam agent. Temperature was regulated via a water-filled stainless-steel base, and the fermenter was equipped with pH and dissolved oxygen sensors (Mettler Toledo). Process parameters during fermentation were controlled (Secure Cell) at 37°C (before induction), pH 7.0 using 1% phosphoric acid and 1 M sodium hydroxide, and $pO_2 \ge 35 \%$ using a sequential cascade of agitation between 250 and 800 rpm and pressure air aeration between 2 and 30 L min⁻¹. Expression in small scale flasks as well as large scale fermentation cultures was induced with 0.1 mM isopropyl β -D-1-thiogalactopyranoside (IPTG) when the culture reached OD600 = 0.6, and the temperature was changed to 30°C. After overnight expression, cells were harvested by centrifugation for 15 min at 4500 g at 4°C and stored at -20°C until further processing.

For purification of target proteins, the cell mass was first resuspended in lysis buffer (20 mM Tris, 100 mM NaCl, 8 M urea, pH 8.0) supplemented with DNase, and lysis was performed using a French press (one passage at 2000 psi). The supernatant was applied to a HisTrapTM FF crude column for Ni-NTA chromatography purification using an automated purification system, taking advantage of the attached His6-tag. To that end, the column was first washed with three column volumes (CV) of lysis buffer supplemented with imidazole (15 mM) to elute nonspecifically bound protein. The target protein was then eluted with 3 CV of lysis buffer containing 300 mM imidazole. Individual elution fractions were pooled after assessment by sodium dodecyl sulfate-polyacrylamide gel electrophoresis (SDS-PAGE) and dialyzed overnight at 4°C against 2% acetic acid (molecular weight cut off MWCO=10 kDa). Afterwards, the protein solution was centrifuged to remove precipitates. The sample was concentrated using cen-

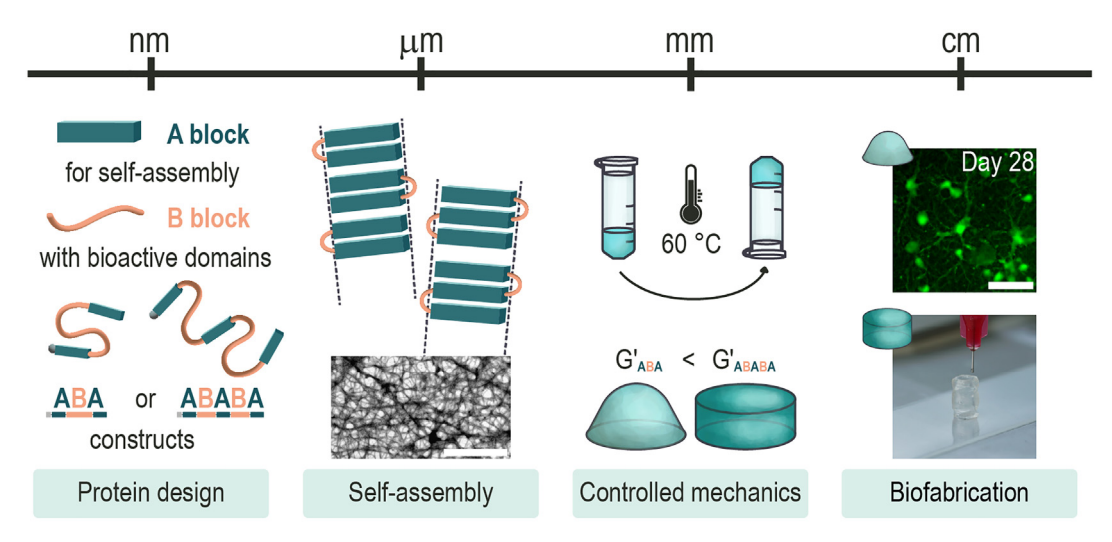


Fig. 1. Bottom-up design of a modular protein platform. Left (Protein design): The design of modular protein hydrogels starts from the structure of self-assembling (A block) and biomolecule binding (B block) domains. Center left (Self-assembly): These domains are combined within distinct polymers, the 183 amino acid-long ABA and the 258 amino acid-long ABABA, that self-assemble under suitable conditions to form fibrillar networks. Center right (Controlled mechanics): The fibrillar networks result in hydrogel biomaterials with tunable mechanics. Right (Biofabrication): The mechanical properties of the hydrogels can be tailored for biofabrication of soft substrates (e.g., for neuron tissue model, cortical neurons cells stained in green) and of stiff 3D constructs (e.g., high profile tubular scaffolds). Scale bars, left: 1 µm, right: 50 µm.

trifugal filters, and the concentration of the purified proteins was determined in solution at 280 nm (NanoDrop, Thermo Scientific) according to Beer's Law, using the respective molecular weight and extinction coefficients.

Purified protein samples were measured by MALDI-MS. A saturated solution of sinapinic acid in acetonitrile and 0.1% trifluoroacetic acid solvent mixture was used as a MALDI matrix. Finally, 1 μ L of the sample matrix solution was deposited on a stainless steel plate and allowed to dry at room temperature. Measurements were performed with a MALDI-TOF mass spectrometer (AutoflexSpeed, Bruker Daltonics) equipped with a solid state Nd:YAG laser emitting at 355 nm wavelength. Spectra were acquired monitoring a mass range 5 – 20 kDa in linear positive mode using Flex-Control 3.0 software (Bruker Daltonics).

2.3. Self-assembly and characterization of the designed modular proteins

Self-assembled protein samples were prepared from protein stock solutions in 2 % acetic acid. The final protein concentration (4 – 130 mg mL $^{-1}$) was adjusted by centrifugal filtration (Amicon Ultra-0.5 mL Centrifugal Filters, Merck) at 14,000 rcf for 2 – 15 min. The samples were then transferred to dialysis units (Micro Float-A-Lyzer, MWCO=0.5 – 1.0 kDa, Repligen) and placed in a PEG (M $_{\rm n}\sim$ 8000 Da, ref. 89510, Sigma) solution in milliQ water to match the osmotic pressure of the protein solution. The dialysis solution was changed twice every 12 h to reach a final pH of \sim 6. After recollection, the final protein concentration was measured using NanoDrop and data were binned with other samples within a range of 5 mg mL $^{-1}$.

Protein samples prepared from lyophilized protein solutions at 1 mg mL⁻¹ (below the gelation concentration) and 10 mg mL⁻¹ (above the gelation concentration) before and after heat treatment at 60°C were used to assess protein conformation by attenuated total reflectance Fourier transform infrared spectroscopy (ATR-FTIR, Spectrum Two, PerkinElmer) with 1 cm⁻¹ resolution and performing 32 scans for each measurement. Protein solutions (1 and 4 mg mL⁻¹) after self-assembly were investigated using transmission electron microscopy (TEM, FEI Morgagni 268) after staining with 2% uranyl acetate (described in detail in the Supplementary Infor-

mation). The narrowest identifiable fibers were manually measured (n=150) using ImageJ.

2.4. Characterization of hydrogel gelation and final mechanical properties

To prepare hydrogel samples for scanning electron microscopy (SEM, JOEL JSM 7100F) imaging, $110-120~{\rm mg~mL^{-1}}$ protein solutions were gelled at $60^{\circ}{\rm C}$ for 90 min. The hydrogels were cast in a well plate and crosslinked in 2.5% glutaraldehyde for 30 min (Fig. S1), dehydrated with ethanol of increasing concentrations, and dried using critical point dryer (CPD 931, Tousimis).

Rheological measurements of protein gelation were performed using a strain-controlled shear rheometer (MCR 502; Anton-Paar) with a Peltier stage and a sandblasted plate-plate ($\emptyset = 8 \text{ mm}$) geometry. The experiments were performed at 60°C for 90 min at a constant angular frequency ($\omega = 10 \text{ rad s}^{-1}$) and constant shear strain ($\gamma = 0.3\%$). Silicone oil was used to isolate the sample during the test to prevent drying. The same rheometer configuration was used to perform oscillatory frequency sweep experiments $(\gamma = 0.3\%)$ at room temperature (25°C) to determine the viscoelastic behavior of the hydrogels. Storage modulus values at angular frequency $\omega = 10 \text{ rad s}^{-1}$ were used to compare samples. A measuring gap of 0.3 - 0.6 mm was used to ensure that the ratio between the measuring gap and protein fibril width was at least 10 (based on the practical guideline provided by Anton Paar) while a torque of at least 50 nN·m was recorded for oscillatory shear measurements (Fig. S2).

2.5. Cell attachment studies

Two cell types from different tissues were used to evaluate cell attachment. The NIH/3T3 fibroblast cell line (CRL-1658, ATCC) was cultured in Dulbecco's modified Eagle's medium (DMEM, ref. 31966-021, ThermoFisher) supplemented with 10% bovine serum (BS, ref. 16170078, ThermoFisher) and 1% penicillin-streptomycin (PenStrep; ref. 15140-122, ThermoFisher). C2C12 mouse myoblast cells were cultured in DMEM (ref. 10313-021, ThermoFisher), supplemented with 10% fetal bovine serum (FBS, ref. 10270106, ThermoFisher), 1% GlutaMAX (ref. 35050061, ThermoFisher), 1% non-

essential amino acids (ref. 11140050, ThermoFisher), 1% PenStrep, and 0.05% β -mercaptoethanol (ref. 21985-023, ThermoFisher).

Both cell types were cultured in a 5% CO₂ incubator at 37°C. Trypsin-EDTA solution (ref. 25200-056, ThermoFisher) was used for cell passaging. Cell attachment was studied using medium where serum volume was replaced with PBS with or without additional supplements i.e., soybean trypsin inhibitor (final concentration 1 mg mL⁻¹, ref. T6522, Sigma) or CRGDS (further RGD, 10 mM final concentration, GenScript). Cells (5,000 cells per well) were seeded in a 96 well plate coated with 15 mg mL⁻¹ protein gels (blocked with 1% bovine serum albumin at 4°C overnight) for 30 min. The samples were then washed with Hank's Balanced Salt Solution (HBSS, ref. 14025092, ThermoFisher) 2 times and fixed using 4 %formaldehyde solution (ref. 100496, Sigma) for 15 min. The actin filaments (Phalloidin-iFluor 488, ref. ab176753, Abcam) and cell nuclei (DAPI, ref. D9542, Sigma) were stained according to manufacturer instructions and the samples were imaged using an inverted wide field fluorescence microscope (THUNDER Live Cell; Leica) using an HC PL FLUOTAR L 40x/0.6 corr Ph2 objective. Image analysis was performed using CellProfiler 4.2.5 (described in detail in the Supplementary Information). All experiments were performed with a minimum of three replicates and n = 50 cells were used to evaluate cell spreading for each condition.

2.6. Cortical neuron culture

Primary cortical neurons were obtained from the cerebral cortices of embryos (E18) of time-mated Wistar rats (Harlan Laboratories, Netherlands). All animal experiments were approved by the Cantonal Veterinary Office of Zurich. Briefly, the cortices were dissociated at 37°C, by adding 5 mL of a filter-sterilized solution of papain (ref. P4762, Sigma), at a concentration of 0.5 mg mL^{-1} . After 15 min, the supernatant was removed and the solution was washed with complete neurobasal medium [NBM (ref. 21103049, ThermoFisher) supplemented with 2% B27 (ref. A3582801, Thermofisher), 1% Glutamax (ref. 35050087, ThermoFisher), and 1% PenStrep] with 10% FBS. After 5 min, the supernatant was removed and the samples were washed twice with complete NBM for 5 min each. After the third wash, the tissue sections were triturated with a 1000 µL pipette and the cells were counted. For culturing of the cells, 20 μL of 15 mg mL^{-1} protein hydrogels were deposited in a 96-well plate. Poly-D-lysine (PDL, ref. P7280, Sigma) coated well plates were used as a positive control. 30,000 cells per well were seeded on each protein hydrogel which were pre-incubated with complete NBM cell culture medium. Every 3 - 4 days, half of the media was replaced with fresh complete NBM, LIVE/DEAD (ref. L-3224, ThermoFisher) staining was used to monitor cell viability. After 14 and 28 days of culture, samples were fixed using 4% formaldehyde solution for 10 min. After three washes with PBS (5 min each), the samples were stored at 4°C in PBS until ready for

Next, a 0.1% solution of TritonX-100 (ref. T8787, Sigma) in PBS was added to each well for 6 min followed by 6 washes with a blocking buffer [5% goat serum (ref. G9023, Sigma) in PBS]. Then, the primary antibody Tuj1 (ref. ab18207, Abcam) was added at a 1:1000 dilution in PBS and incubated at 4°C overnight. The next day, the primary antibody solution was removed and the samples were rinsed 6 times with the blocking buffer. A secondary antibody, goat anti-rabbit Alexa 647 (A-21245, Invitrogen, ThermoFisher) was added at a 1:300 dilution and left for 1 h to incubate at room temperature in the dark. Next, the samples were washed twice and a 1:500 dilution of Hoechst (ref. 63493, Sigma) in PBS was added to each well and incubated for 10 min. After two more washes with PBS, the samples were stored in fresh PBS. Fluorescence microscopy images were collected using a confocal laser scanning microscope (FluoView FV3000, Olympus). The sam-

ples were imaged using an UPLFLN20XPH (Universal Plan Fluorite) 20x/ 0.50 Ph1 objective.

2.7. Biofabrication experiments

Direct ink writing was performed using a pneumatic 3D printer (Bio X, CELLINK). The scaffolds were designed using Rhino (version 7, Robert McNeel & Associates) software. 40 – 50 mg mL $^{-1}$ ABABA protein hydrogels were extruded through 25G nozzle (d = 250 mm) using printing speed of $v_{printing}=3$ – 4 mm s $^{-1}$; and pressure $P_{extrusion}=35$ – 55 kPa and 27G nozzle (d = 200 mm) using $v_{printing}=8$ – 16 mm s $^{-1}$; and pressure $P_{extrusion}=69$ – 80 kPa.

Circular porous scaffolds were printed for culturing bone marrow derived human mesenchymal stromal cells (hMSCs) isolated from healthy donors during orthopedic procedures with informed consent in accordance with the local ethical committee (University Hospital Basel; Prof Kummer; approval date 26 March 2007, Ref Number 78/07) [37]. Prior to the experiment, the cells were cultured in MEM alpha cell culture medium (ref. 22561021, ThermoFisher) supplemented with 1% PenStrep, 5 ng mL⁻¹ bFGF, and 10% FBS incubated at 37°C, 5% CO₂. The printed scaffolds were washed with medium for 1 h and then 10,000 cells per scaffold were seeded. For osteogenic differentiation, MEM alpha supplemented with 1 % PenStrep, 10% FBS, 0.05 mg mL⁻¹ ascorbic acid (ref. A4544, Sigma), 10 mM beta glycerophosphate (ref. G9422, Sigma), 10 mM HEPES (ref. H4034, Sigma), 1 mM sodium pyruvate (ref. 11360039, ThermoFisher), 2 mM L-glutamine (ref. 25030024, ThermoFisher), and 100 ng mL⁻¹ bone morphogenic factor BMP-2 (ref. 120-02C, PeproTech) was used and changed every 3 - 4 days [38]. Media without BMP-2 as well as normal hMSC media were used as controls. To evaluate alkaline phosphatase activity, the samples were washed once with PBS and then incubated with SIGMAFASTTM BCIP®/NBT (ref. B5655, Sigma) solution for 20 min. They were then washed twice with PBS and fixed with 4% formaldehyde solution for 30 min. The samples were imaged using an EVOS cell imaging system (ThermoFisher). Protein hydrogels were stained using Amytracker680 (Ebba Biotech) according to the manufacturer's instructions. In addition, actin filaments and cell nuclei were stained and imaged as previously described in section 2.5.

2.8. Data analysis and statistics

Data fitting and statistical analysis was performed using OriginPro 2019 software. Student's t-test was performed to compare the means between the sample groups. Differences were considered statistically significant at a level of *** p=0.001.

3. Results

3.1. Modular protein design and expression

To control hydrogel properties, we employed a modular design approach combining distinct self-assembly domains, bioactive motifs, and flexible hydrophilic linkers in two individual polymer chains, the 183 amino acid-long ABA and the 258 amino acid-long ABABA constructs (Fig. 2A; for full sequences, see Table S1). For successful production and subsequent hydrogel formation, the amino acid compositions of the complete proteins were designed to balance self-assembly propensity and aqueous solubility. To achieve this, we used an alternating AB block copolymer architecture, as this design has proven useful to generate a variety of functional materials including peptide-based hydrogels [39].

For the self-assembly domain (A block), we used 2.5 repeats of the EAK-16 peptide (AEAEAKAKAEAEAKAK; A – alanine, E – glutamic acid, K – lysine). The EAK-16 peptide was originally identi-

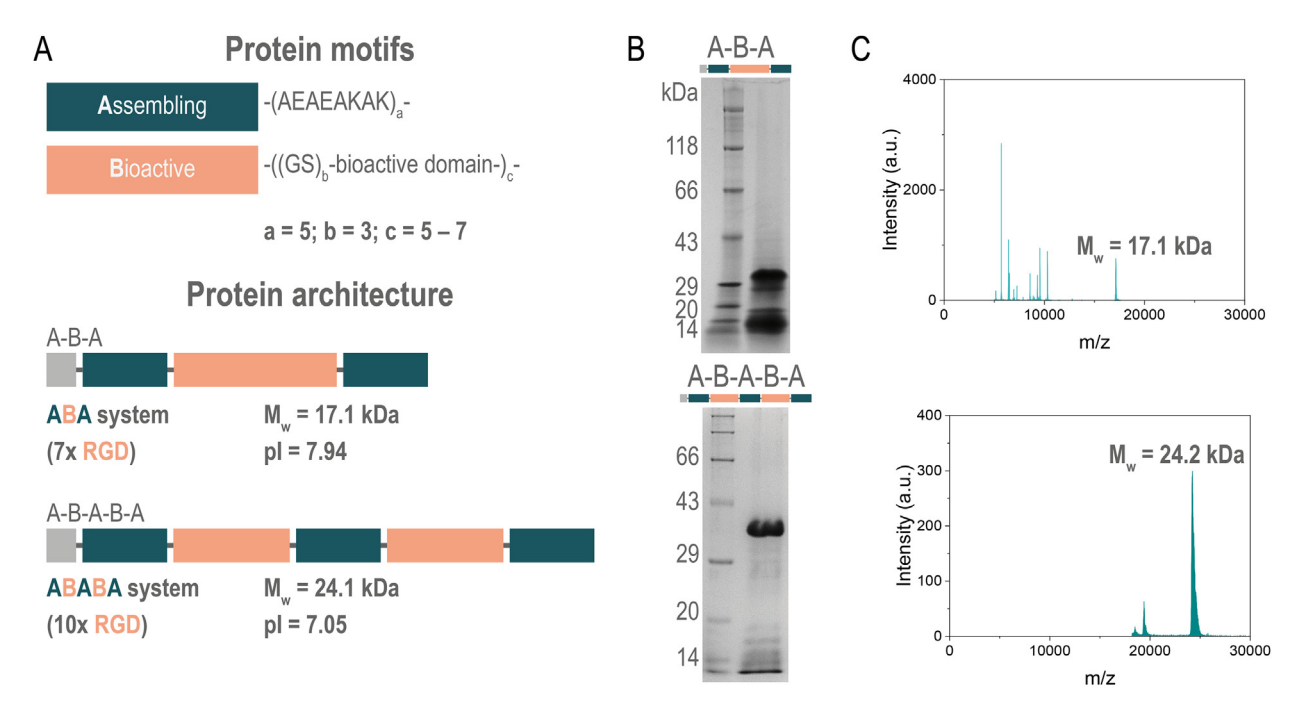


Fig. 2. Modular protein design and expression. A: Self-assembly domains (A block) and bioactive domains (B block) were used to engineer ABA and ABABA proteins. The grey block in each protein represents the N-terminal hexahistidine tag used for purification. Full sequences are provided in the ESI, Table S1. Expression of ABA (top) and ABABA (bottom) proteins confirmed by B: SDS-PAGE and C: MALDI-MS.

fied as a tandem repeat in the nucleic acid binding protein Zuotin [40] and has been shown to form stable beta-sheets that can further assemble to produce hydrogels [41,42]. Further, EAK peptides, and their derivatives, can be functionalized with biomimetic motifs, for example to enable cell adhesion [43]. However, besides hydrogels generated from a nonamer of EAK-16 [44], studies on protein hydrogels based on this peptide have been limited. In the present work, we combined multiple EAK domains (A block) within the same polymer via flexible linkers (B block) forming the ABA and ABABA proteins.

The use of flexible linkers to connect multiple self-assembling domains has been successfully employed with coiled-coil forming peptides [45], WW (W – tryptophan) and proline-rich peptide domains [46], and fluorescent sensor proteins [47]. For the linker (B block) used in this work, we chose glycine (G) and serine (S) repeat units as they are well suited to provide both flexibility and aqueous solubility [48]. Furthermore, the linker domains offer ideal sites to introduce bioactive sequences without interfering with the self-assembling blocks. Bioactive RGD (R – arginine, G – glycine, D – aspartic acid) cell-attachment motifs were included in the linker structure to separate them from the self-assembling domains and increase their accessibility in the resulting hydrogels.

Expression of the synthetic genes encoding the designed proteins was performed at 30°C using TB medium either in shake flasks or in batch reactors to provide sufficient quantities of material for protein characterization and subsequent experiments. The yield for pure ABA was 8-10~mg g (wet cell weight (wcw)) $^{-1}$ or 250-350~mg L $^{-1}$, whereas for ABABA it was 1-2~mg g (wcw) $^{-1}$, or 40-80~mg L $^{-1}$ culture, respectively. It is important to note that the expression process has not been optimized. Substantial potential for improvement of the yield lies in the refinement of the fermentation conditions regarding media and temperature or applying fed-batch processes. For comparison, in the case of the recombinant honeybee silk structural protein, a yield of about 2500 mg L $^{-1}$ culture was obtained after optimization [49]. ABA and ABABA proteins were purified by Ni-NTA chromatography. SDS-PAGE analysis confirmed the successful purification of the target proteins,

in addition to some low-molecular weight contaminants (potentially monomer A or dimer AB units) (Figs. 2B and S3). MALDI-MS confirmed the expected molecular weight of the target proteins (Fig. 2C). The resulting ABA and ABABA protein masses were 17.1 kDa and 24.2 kDa respectively, which is in good agreement with the theoretical protein masses of 17.1 kDa and 24.1 kDa, despite an apparent higher molecular weight being observed in the SDS-PAGE analysis.

3.2. Fibrillar network formation via self-assembly of the designed modular proteins

Environmental conditions, such as temperature and pH as well as ionic composition of the solution can promote self-assembly of protein secondary structures [43]. In this work, we used elevated temperature (T = 60°C for 1 h) to induce conformational changes after protein solutions of pH 5.5 - 6.5 were prepared via dialysis [50]. We investigated the physicochemical nature of the materials following self-assembly to understand the formation of secondary and tertiary protein structures. ATR-FTIR was performed on low concentration samples (1 mg mL⁻¹) before and after heat treatment to compare the protein secondary structures (Figs. 3 and S4). Increase in the intensity associated with the amide I peak at 1623 cm⁻¹, indicative of fibrillar beta-sheet structures, was observed in the heat-treated samples [51], whereas a peak at 1650 cm⁻¹, indicating disordered structures [52], was more prominent in the samples prior to heat treatment. The latter peak remained after the heat treatment possibly due to only partial self-assembly of the proteins. The FTIR results indicating an increase in beta-sheet structure were supported by circular dichroism measurements (Fig. S5). This suggested that, upon heating, the ABA and ABABA proteins assembled by formation of fibrillar beta-sheet structures.

To further assess the structures formed during self-assembly, low concentration protein solutions (1 mg mL $^{-1}$) were treated with the same heating process and the resulting sample was imaged with TEM (Figs. 3B, S6–S8). The width of the narrowest identifiable fibers was determined to be 3.2 \pm 0.5 nm and 3.5 \pm 0.7

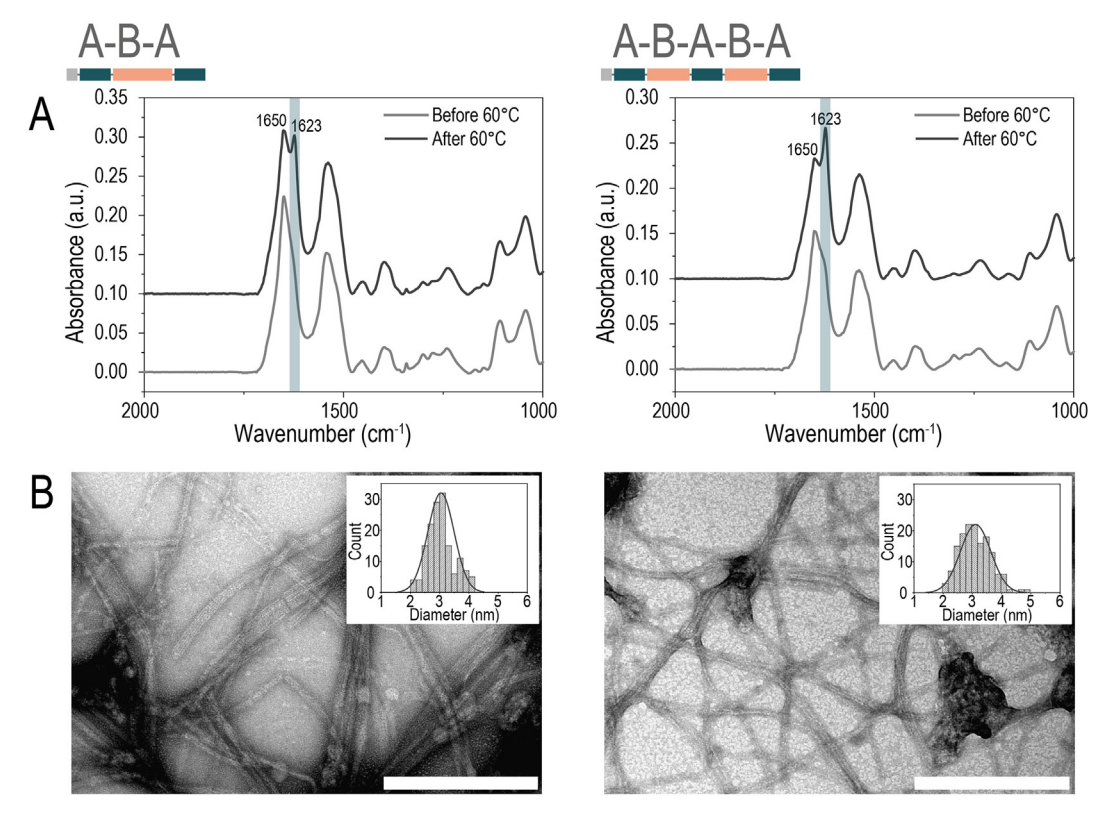


Fig. 3. Protein self-assembly at elevated temperature. A: ATR-FTIR spectra of lyophilized 1 mg mL⁻¹ ABA and ABABA protein samples before and after self-assembly at 60°C. B: TEM images of 1 mg mL⁻¹ ABA (left) and 1 mg mL⁻¹ ABABA (right) self-assembled protein fibril bundles and the distribution of the width of narrowest identifiable fibers (inset). Scale bars, 200 nm.

nm for the ABA and ABABA proteins, respectively. These narrow diameter fibers were attributed to packing patterns of the ABA and ABABA proteins in the cross-section perpendicular to the direction of fiber axis [53]. Within the samples, these individual fibers appeared bundled into long microfibers for both proteins. Such bundling is beneficial for formation of hydrogel networks with increased modulus compared to networks of individual fibers [54].

3.3. Mechanical properties of designed modular protein hydrogels

The EAK16 peptide sequences that comprised the assembling A block in the designed proteins are known to form dense fibrillar networks to produce hydrogels [44]. After confirming the formation of fibrils, we then compared the ABA and ABABA proteins to evaluate if the self-assembling capacity is enhanced by increasing the number of self-assembling domains.

Firstly, we observed that dense fibrillar networks formed at high concentration ($> 100 \text{ mg mL}^{-1}$) for ABA and ABABA protein hydrogels, making a porous mesh (Figs. 4A and S9). Fiber bundles in networks composed of ABA proteins were less branched than fibers of ABABA proteins.

To further study the differences in self-assembly between ABA and ABABA proteins we studied their gelation at elevated temperature (T = 60° C) (Fig. S10). For this, we investigated the self-assembly process in the absence of additional ions to evaluate the self-assembly capacity of the pure proteins. An initial increase in storage modulus (G') of the protein precursor was observed within the first 5 min at elevated temperature (T = 60° C, Fig. 4B). For all protein concentrations tested ($10 - 50 \text{ mg mL}^{-1}$), the storage moduli measured at 90 min after gelation was initiated were higher for ABABA compared with ABA proteins (e.g., $G'_{ABABA} = 0.4 - 44$ kPa whereas $G'_{ABA} = 0.4 - 3.4$ kPa, Fig. 4C). The difference in storage moduli was more pronounced for concentrations above 30 mg mL⁻¹; in this range the modulus of ABABA gels was one order of

magnitude higher than for ABA formulations. Further, the storage moduli, G', scaled with the protein concentration and followed a power law ($G' \sim c^{\nu}$). The values of the exponential parameter ν of both ABA and ABABA networks fell within the range typically used to describe fibrillar networks. The scaling for ABABA networks ($\nu \leq 2.5$) indicated rigid fibrils as compared with semiflexible fibrils for ABA networks ($\nu \leq 2.2$) [55]. The time required to reach G' = 100 Pa (Fig. 4D) was considered as the gelation initiation point. Based on this parameter, the initial formation of ABABA networks started earlier than ABA networks within the measured concentration range (10-50 mg mL $^{-1}$). Finally, the formed hydrogels maintained their properties after cooling to room temperature (Fig. S11).

3.4. Cell-protein hydrogel interactions

RGD peptides found in fibronectin are commonly used in hydrogel engineering to enable cell attachment as they are recognized by several integrins present on the surface of mammalian cells [56]. The formation of secondary structures in protein hydrogels can affect the accessibility of such cell binding domains. For example, RGD is not exposed in native collagen and only becomes available for integrin binding in the denatured form (gelatin) [57]. To date, cell attachment to beta-sheet based materials, such as recombinant spider silk, has been achieved via incorporation of RGD or other cell-adhesive peptide sequences [58]. One feature of our modular protein design is that the presentation of cell attachment peptides can be decoupled from the network formation domains. To demonstrate the ability of our biopolymers to present cell attachment domains (B blocks) in the gel state, we investigated cell attachment and spreading on ABABA protein substrates. To ensure that the adhesion was specific to RGD epitopes in the ABABA proteins, we added the soluble CRGDS peptide to the cell culture medium to competitively bind to the RGD-specific integrins on the cell sur-

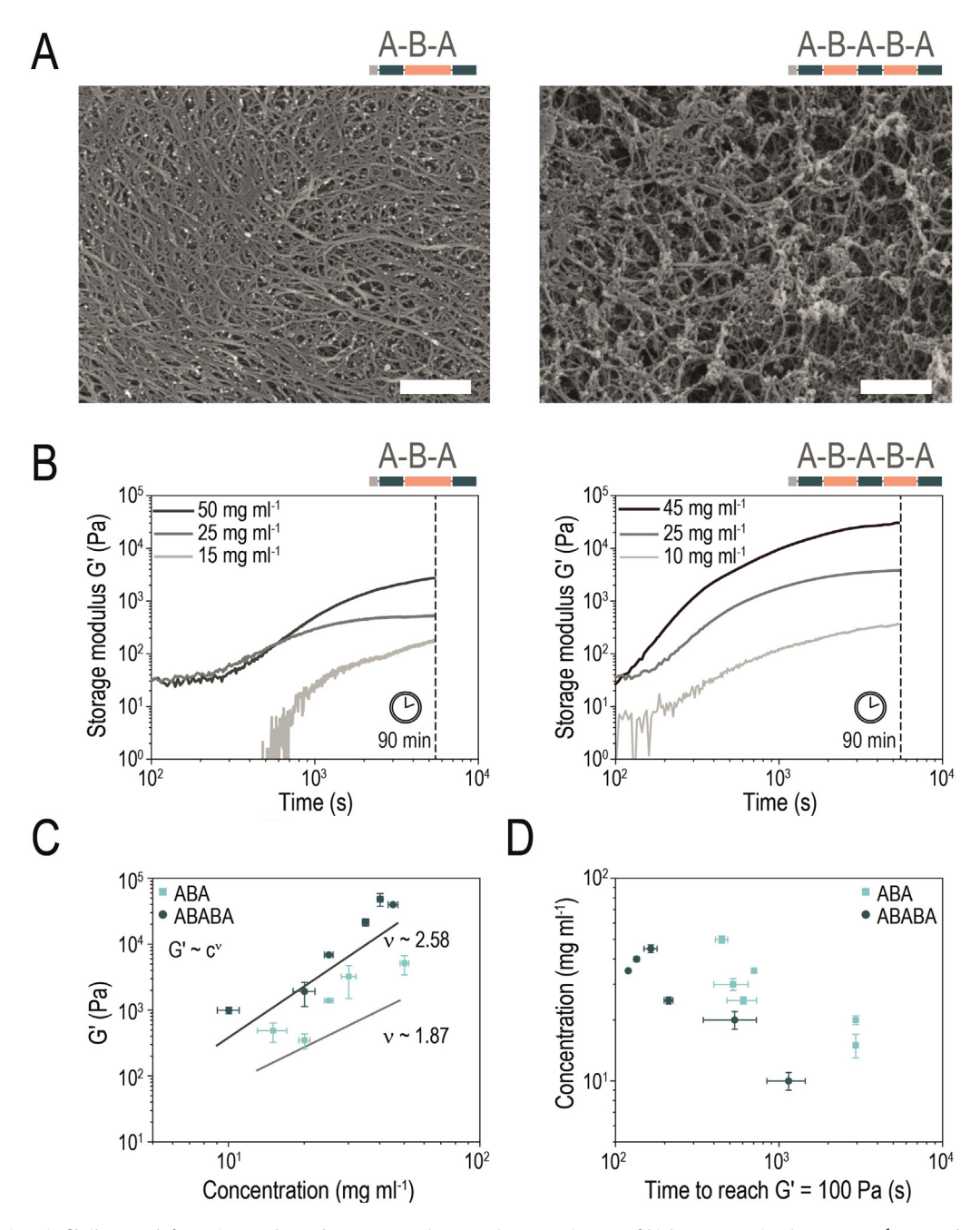


Fig. 4. Protein gelation via fibril network formation at elevated temperature ($T = 60^{\circ}$ C). A: SEM images of high concentration (120 mg mL⁻¹ ABA and 105 mg mL⁻¹ ABABA) protein hydrogels. Scale bar, 1 μm. B: Rheological characterization of gelation kinetics of ABA (left) and ABABA (right) proteins (ω = 10 rad s⁻¹, γ = 0.3 %, and $T = 60^{\circ}$ C). C: Summary of storage moduli G' of protein hydrogels at different protein concentrations after 90 min at 60°C. D: Time required to reach storage moduli G' = 100 Pa for protein solutions of different concentrations.

faces and compared the extent of cell spreading with untreated controls. Finally, we tested the specificity of cell attachment by comparing the attachment of fibroblasts and myoblasts, which differ substantially in their integrin expression.

NIH/3T3 mouse fibroblasts were seeded on the protein hydrogels (15 mg mL $^{-1}$) with and without competitive 10 mM CRGDS peptide in the culture medium. Cell spreading was impaired upon the addition of CRGDS; the mean major axis cell length decreased from 7.5 \pm 3 μ m to 4.2 \pm 1 μ m (Fig. 5A). This indicates that RGD-specific integrins are required for cells to adhere and spread on our modular protein substrates (Fig. 5B).

Additionally, C2C12 mouse myoblast cells were seeded on the protein hydrogels (15 mg $mL^{-1}).$ Again, cell elongation was reduced significantly upon the addition of a competitive, soluble

CRGDS peptide (from 4.5 \pm 2 μm to 3 \pm 1 μm , Fig. 5A), and overall cell spreading was much lower compared to fibroblasts and similar to that of the NIH/3T3 control on tissue culture plastic (Fig. S12). We hypothesized that the impaired cell spreading for C2C12 my-oblasts was due to differential expression of integrins in muscle cells that bind primarily to collagen and laminin in muscle ECM [59].

3.5. Designed modular protein hydrogels for biofabrication of cell culture scaffolds

After confirming that our protein design allowed tunable mechanical properties and presentation of cell adhesion sites after self-assembly, we exploited the ability to tailor cell-material inter-

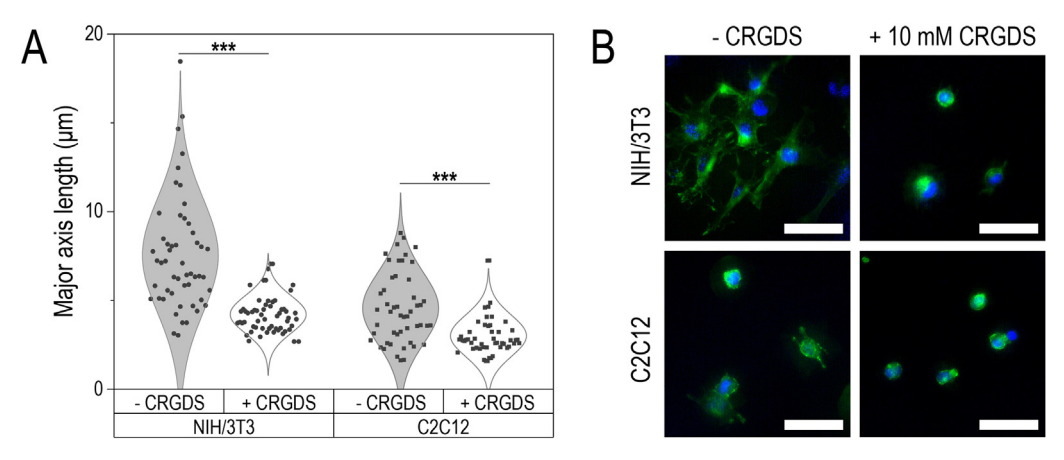


Fig. 5. Cell attachment on protein hydrogels. A: Measurement of major axis length and B: cytoskeleton staining (actin in green, nuclei in blue) of NIH/3T3 and C2C12 cells seeded on 15 mg mL⁻¹ ABABA protein hydrogels with and without 10 mM CRGDS peptide as a competitor for integrin binding. Scale bars, 50 μm.

actions for further studies of cell growth on our engineered protein hydrogels. We investigated whether our fibrillar protein hydrogels could serve as support structures for neuronal cell growth and function. To achieve this, we seeded primary cortical neurons on soft (G' = 0.07 - 0.1 kPa, Fig. S13) ABA and ABABA hydrogels. The cells attached and spread homogeneously on the hydrogel surface, and their viability was maintained for up to 4 weeks (Figs. S14 and S15). After 2 weeks of culture, neurites sprouted and the cells grew in multi-layered structures to form an extensive network as confirmed by beta3-tubulin staining (Fig. 6 A). After 4 weeks, the neurite networks were expansive and spanned the entire surface area of the gel. Given that neurons are sensitive to substrate mechanical properties [60], they were also seeded on stiff ABA and ABABA hydrogels (G' = 5 - 7 kPa, Fig. S13). In this case, most of the cells were not able to maintain contact with the substrate and detached from the surface (Fig. S16). Very few neurites and nuclei were visible at the 4 week timepoint. This confirmed that the neurons responded to protein hydrogel mechanical properties and that cell growth can be achieved by tailoring the hydrogel storage modulus. This agrees with previous studies on bioactive EAK peptide-based fibrillar hydrogels that were reported to support enteric neuron growth [61].

Beyond neuronal cell growth, we used the modular proteins for 3D printing of more complex cell scaffolds. Stiff ABABA hydrogels (45 \pm 2 mg mL⁻¹, storage modulus G' = 5 - 9 kPa, Fig. S17) showed self-healing (75 - 90 % elastic recovery of initial G' after high strain intervals: $\gamma = 100\%$, $\Delta t = 2$ min, $\omega = 10$ rad s⁻¹) and shear-thinning (shear-thinning index n = 0.05 - 0.1) properties that suggested they would be suitable for 3D printing and biofabrication (Fig. S18). Over a course of 35 days extruded hydrogels showed no swelling or degradation which suggested that they would remain stable during long-term cell culture of 3D scaffolds (Fig. S19). The protein-based hydrogel ink was evaluated for printing using direct ink writing (Fig. S20). Multilayered grid structures (27G nozzle (d = 200 mm); $v_{printing} = 7 \text{ mm s}^{-1}$; $P_{extrusion} = 90$ kPa) as well as self-supporting multilayer (n = 40) structures were printed (25G nozzle (d = 250 mm); $v_{printing} = 3 - 4 \text{ mm s}^{-1}$; $P_{extrusion} = 35 - 55$ kPa; Fig. 6B). Printed porous scaffolds were used as substrates for osteogenic differentiation of hMSCs. During the first 2 weeks of culture the cells grew on the surface of the scaffolds and in between the pores (Fig. 6C). Moreover, in BMP-2containing media, alkaline phosphatase (ALP) activity and osteocalcin (OCN) were detected in the population of cells growing on protein hydrogels and attached to the pores of the scaffold (Figs. 6D and S21). After 4 weeks, ALP activity was also detected in cells attached to the printed scaffolds when cultured in differentiation media without BMP-2 (Fig. S22). This illustrated how high modulus protein hydrogels are suitable for digital fabrication of biomaterials and osteogenic differentiation of hMSCs.

4. Discussion

Protein hydrogels offer versatile solutions for a range of biomedical applications, including biofabrication of disease models [25] and delivery of therapeutics [62]. There are two main design approaches to tailor proteins at a molecular scale: modular design [63] and chemical modification [64,65]. Modular design of recombinant proteins provides freedom for the selection of network formation processes and the resulting properties of the hydrogels [18,66,67]. In our work, we incorporated amphiphilic EAKA sequence repeats into self-assembling (A block) domains and combined these with hydrophilic and flexible GS-based linkers containing cell-binding RGD motifs (B blocks). These biopolymers are produced in *E. coli* through heterologous expression and purification, and their yield can be further improved through process optimization.

Using this design, we fabricated both ABA and ABABA proteins, hypothesizing that the self-assembly capacity would be enhanced in an ABABA system as compared to ABA system, given the increased number of assembling domains. The designed proteins exhibited increased beta-sheet structures at elevated temperature (60°C), which resulted in fiber formation and gelation. ABABA proteins formed hydrogels more rapidly and the resulting networks exhibited higher storage modulus for the same concentration as ABA and increased rigidity of the formed fibers (higher scaling of modulus with protein concentration). We hypothesized that the increased number of assembling A domains from 2 to 3 may allow for more efficient network formation as it may increase the possibility of crossover between individual peptides. This is consistent with the increased gelation rate for ABABA samples as compared with ABA samples at a similar concentration, despite the lower molar fraction of assembling domain, and the increased modulus for ABABA samples. One unexplored consideration in the current work that merits future investigation is the potential role of polymer entanglement during the heating process, which may influence gelation. Additional measurements, such as AFM in liquid environment, would allow further understanding of the differences between the formed fibrils and their networks. The increase in fibril formation rate with additional assembling domains is consistent with observations in spider silk, where fiber nucleation and growth were enhanced with increasing number of β -sheet forming segments [68]. Moreover, in the context of replicating the viscoelastic behavior of fibrillar ECM constituents it is beneficial to have a library of fibers with varying degrees of rigidity, which can

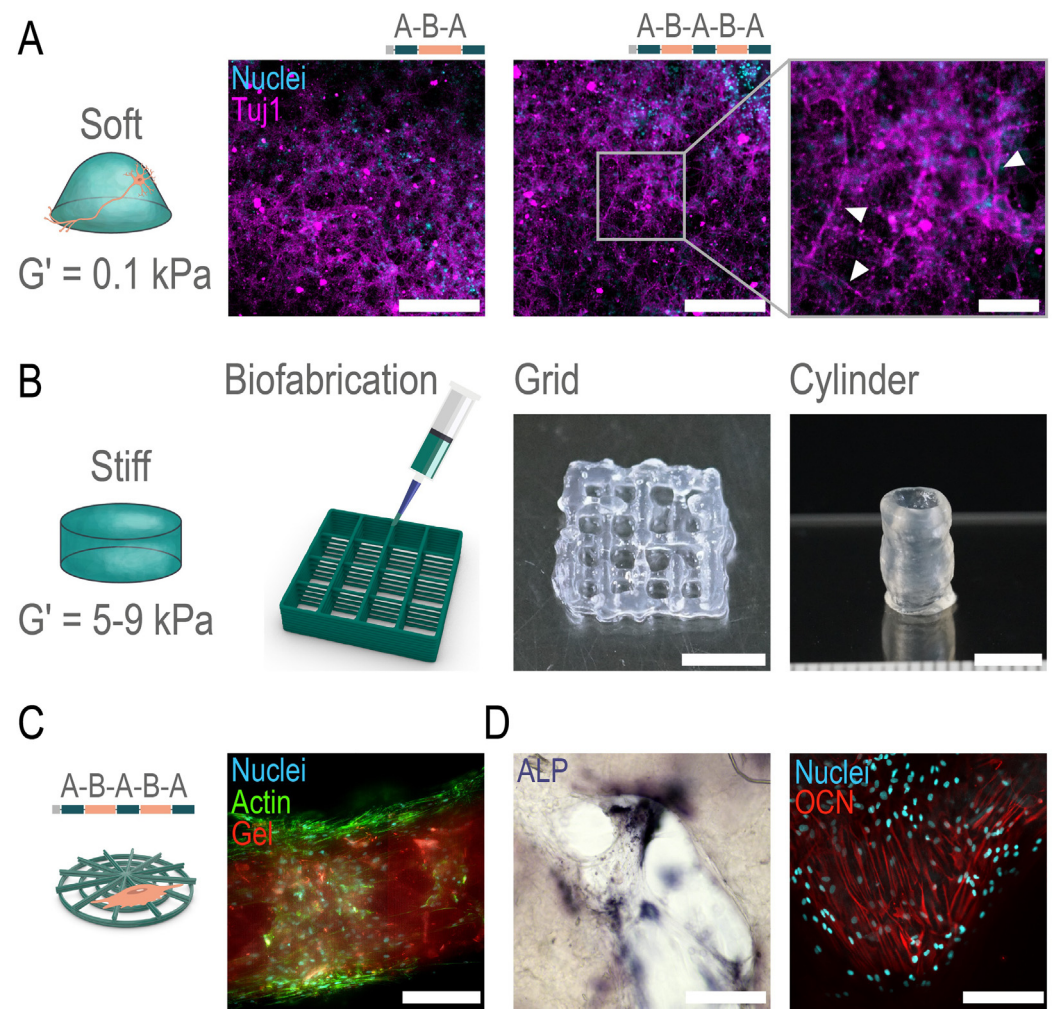


Fig. 6. Biofabrication of designed modular protein hydrogel scaffolds. A: Beta3 tubulin (Tuj1) staining of neuron cells after 14 days of culture on soft ABA and ABABA protein hydrogels (G' = 0.07 - 0.1 kPa), Tuj1 (magenta), nuclei (cyan). B: Direct ink writing of protein inks into porous 3D structures. C: hMSCs spreading on porous scaffolds (red) after 2 weeks of cultivation actin (green) nuclei (blue), D: ALP (left image, purple) and osteocalcin (right image, OCN, red) stainings indicating osteogenic differentiation of hMSCs on protein hydrogel scaffolds. Scale bars, A left and middle: 200 μm, right: 50 μm; B 5 mm; C 200 μm; D left: 300 μm, right: 200 μm.

be controlled by altering the number of repeating self-assembling domains per molecule. Another consideration for the use of these materials is the potential presence of low molecular weight contaminants. In this work, we did not observe any adverse affects of unpurified peptide sequences on fiber formation, mechanical properties, or cell viability; however, further purification procedures could lead to improved materials performance.

To address the importance of cell attachment sites in hydrogel platforms for tissue engineering, we demonstrated that cells engage and spread on protein hydrogels and confirmed the availability of cell adhesion sites within B blocks after protein selfassembly. The accessibility of the RGD sequence opens possibilities to include synergistic sites [69], integrin attachment domains for different types of integrins [58], matrix metalloprotease degradation sequences [70], and sites that mimic biomolecule activity [71,72], bind them [73,74], or control their delivery [75]. In addition, modular protein design may allow independent tuning of the bioactivity of the proteins without impacting the mechanical properties of the fibers. While generally stable [76], the degradation products of beta-sheet based protein fibrils or the repetitive sequences in our polymers may stimulate short- or long-term immune signaling, which could limit direct application of these scaffolds in vivo. However, this same feature could be exploited to engineer immune-activating biomaterials for applications in materialbased vaccines or cancer immunotherapy. Further, fibrillar peptide hydrogels can be used for sustained release of growth factors and monoclonal antibodies, as well as for wound healing applications [77].

Another application of our materials is their use as scaffolds for cell culture or biomaterial inks for additive manufacturing. Biofabrication of peptide and protein hydrogels often poses challenges, especially in balancing the processability of the materials performance as static scaffolds, injectable materials, or as inks for 3D printing. In this work, soft protein hydrogels were suitable substrates to support the viability and network formation of cortical neurons for up to four weeks. In the case of 3D printing, the mechanical properties of protein hydrogel inks can be sufficient for both extrusion-based processing as well as shape retention post-printing. Various strategies from protein engineering [34] to printing with support materials [78] have been employed to enable printing with this class of materials. In our work, we exploited the fibrillar nature of the hydrogels to flow upon applied pressure while maintaining the printed porous structure after exiting the syringe. The possibility of using the same protein hydrogel to meet the biological and mechanical requirements for wide range of biofabrication applications makes these hydrogels an attractive solution for creation of 3D cell-laden constructs.

5. Conclusion

In this work we employed a modular protein design approach to form supramolecular fibrillar hydrogels. The self-assembly behavior and mechanical properties of these hydrogels are dependent on protein architecture and concentration. We demonstrated that the resulting fibrillar hydrogels can be applied as soft scaffolds for the growth of neurons and as stiffer scaffolds for the osteogenic differentiation of human mesenchymal stem cells (hMSCs). Overall, these materials provide a promising avenue for the development of cell culture platforms suitable for tissue engineering applications. Moreover, these protein hydrogels can be used as protein hydrogel inks to fabricate porous 3D structures. The modular design with bioactive domains enables the inclusion of other functional motifs, such as degradation sequences or drug-binding sites, opening the possibility for these materials to be used in controlled drug delivery or regenerative medicine applications.

Declaration of competing interest

The authors declare the following financial interests/personal relationships which may be considered as potential competing interests:

TGWE, YO, MH, DD, EAG, ZRN, CP, MWT, and DH are listed as co-inventors of a provisional patent application on the materials described in this manuscript.

Acknowledgments

The project was funded by Innosuisse Impulse [35545.1 IP-LS] and the Swiss National Science Foundation [200021_184697]. The authors acknowledge the ScopeM facility and especially Dr. Anne Greet Bittermann for her help with sample preparation for SEM imaging; Prof. Dr. Raffaele Mezzenga from Laboratory of Food and Soft Materials at ETH Zurich for support with circular dichroism measurements; Prof. Dr. Ivan Martin at the University Hospital Basel for providing the hMSCs; Prof. Dr. Ori Bar-Nur from Laboratory of Regenerative and Movement Biology at ETH Zurich for providing the C2C12 cells; Dr. Lisa Krattiger from Ehrbar Lab at University Hospital Zurich for support in cell culture experiments; Laboratory of Biosensors and Bioelectronics at ETH Zurich for support in neuron experiments and access to confocal microscope; Dr. Ivana Kroslakova (ZHAW) for MALDI service; Dr. Céline Labouesse for valuable discussions regarding cell-material interactions.

Supplementary materials

Supplementary material associated with this article can be found, in the online version, at doi:10.1016/j.actbio.2024.02.019.

References

- [1] A.M. Rosales, K.S. Anseth, The design of reversible hydrogels to capture extracellular matrix dynamics, Nat. Rev. Mater. 1 (2016), doi:10.1038/natrevmats.
- [2] J. Li, D.J. Mooney, Designing hydrogels for controlled drug delivery, Nat. Rev. Mater. 1 (2016), doi:10.1038/natrevmats.2016.71.
- [3] A.P. Mathew, S. Uthaman, K.H. Cho, C.S. Cho, I.K. Park, Injectable hydrogels for delivering biotherapeutic molecules, Int. J. Biol. Macromol. 110 (2018) 17–29, doi:10.1016/j.ijbiomac.2017.11.113.
- [4] J. Li, L. Mo, C.H. Lu, T. Fu, H.H. Yang, W. Tan, Functional nucleic acid-based hydrogels for bioanalytical and biomedical applications, Chem. Soc. Rev. 45 (2016) 1410–1431. doi:10.1039/c5cs00586h.
- [5] A.K. Means, M.A. Grunlan, Modern strategies to achieve tissue-mimetic, mechanically robust hydrogels, ACS Macro Lett. 8 (2019) 705–713, doi:10.1021/ acsmacrolett.9b00276.
- [6] S.A. Fisher, A.E.G. Baker, M.S. Shoichet, Designing peptide and protein modified hydrogels: selecting the optimal conjugation strategy, J. Am. Chem. Soc. 139 (2017) 7416–7427, doi:10.1021/jacs.7b00513.

- [7] E. Gazit, Self-assembled peptide nanostructures: the design of molecular building blocks and their technological utilization, Chem. Soc. Rev. 36 (2007) 1263– 1269. doi:10.1039/b605536m.
- [8] C.M. Elvin, A.G. Carr, M.G. Huson, J.M. Maxwell, R.D. Pearson, T. Vuocolo, N.E. Liyou, D.C.C. Wong, D.J. Merritt, N.E. Dixon, Synthesis and properties of crosslinked recombinant pro-resilin, Nature 437 (2005) 999–1002, doi:10.1038/ nature04085.
- [9] A. Fernández-Colino, F.J. Arias, M. Alonso, J.C. Rodríguez-Cabello, Self-organized ECM-mimetic model based on an amphiphilic multiblock silk-elastin-like corecombinamer with a concomitant dual physical gelation process, Biomacromolecules 15 (2014) 3781–3793, doi:10.1021/bm501051t.
- [10] W. Sun, T. Duan, Y. Cao, H. Li, An injectable self-healing protein hydrogel with multiple dissipation modes and tunable dynamic response, Biomacromolecules 20 (2019) 4199–4207, doi:10.1021/acs.biomac.9b01114.
- [11] K. Schacht, T. Scheibel, Controlled hydrogel formation of a recombinant spider silk protein, Biomacromolecules 12 (2011) 2488–2495, doi:10.1021/ bm200154k.
- [12] W. Liu, K. Merrett, M. Griffith, P. Fagerholm, S. Dravida, B. Heyne, J.C. Scaiano, M.A. Watsky, N. Shinozaki, N. Lagali, R. Munger, F. Li, Recombinant human collagen for tissue engineered corneal substitutes, Biomaterials 29 (2008) 1147– 1158, doi:10.1016/j.biomaterials.2007.11.011.
- [13] Q. Bian, L. Fu, H. Li, Engineering shape memory and morphing protein hydrogels based on protein unfolding and folding, Nat. Commun. 13 (2022) 137, doi:10.1038/s41467-021-27744-0.
- [14] R. Vegners, I. Shestakova, I. Kalvinsh, R.M. Ezzell, P.A. Janmey, Use of a gelforming dipeptide derivative as a carrier for antigen presentation, J. Pept. Sci. 1 (1995) 371–378, doi:10.1002/psc.310010604.
- [15] J.P. Schneider, D.J. Pochan, B. Ozbas, K. Rajagopal, L. Pakstis, J. Kretsinger, Responsive hydrogels from the intramolecular folding and self-assembly of a designed peptide, J. Am. Chem. Soc. 124 (2002) 15030–15037, doi:10.1021/ia027993g.
- [16] W.A. Petka, J.L. Harden, K.P. McGrath, D. Wirtz, D.A. Tirrell, Reversible hydrogels from self-assembling artificial proteins, Science 281 (1998) 389–392, doi:10.1126/science.281.5375.389.
- [17] S. Das, D. Das, Rational design of peptide-based smart hydrogels for therapeutic applications, Front. Chem. 9 (2021) 770102, doi:10.3389/fchem.2021.770102.
- [18] A.M. Kushner, Z. Guan, Modular design in natural and biomimetic soft materials, Angew. Chem. Int. Ed. 50 (2011) 9026–9057, doi:10.1002/anie.201006496.
- [19] W.B. Zhang, F. Sun, D.A. Tirrell, F.H. Arnold, Controlling macromolecular topology with genetically encoded SpyTag-SpyCatcher chemistry, J. Am. Chem. Soc. 135 (2013) 13988–13997, doi:10.1021/ja4076452.
- [20] J.C. Liu, S.C. Heilshorn, D.A. Tirrell, Comparative cell response to artificial extracellular matrix proteins containing the RGD and CS5 cell-binding domains, Biomacromolecules 5 (2004) 497–504, doi:10.1021/bm034340z.
- [21] W. Liu, S. Wong-Noonan, N.B. Pham, I. Pradhan, A. Spigelmyer, R. Funk, J. Nedzesky, H. Cohen, E.S. Gawalt, Y. Fan, W.S. Meng, A genetically engineered Fc-binding amphiphilic polypeptide for congregating antibodies in vivo, Acta Biomater. 88 (2019) 211–223, doi:10.1016/j.actbio.2019.02.037.
- [22] L. Li, Z. Tong, X. Jia, K.L. Kiick, Resilin-like polypeptide hydrogels engineered for versatile biological functions, Soft Matter 9 (2013) 665–673, doi:10.1039/ C2SM26812D.
- [23] A. Girotti, D. Orbanic, A. Ibáñez-Fonseca, C. Gonzalez-Obeso, J.C. Rodríguez-Cabello, Recombinant technology in the development of materials and systems for soft-tissue repair, Adv. Healthc. Mater. 4 (2015) 2423–2455, doi:10.1002/adhm.201500152.
- [24] R. Mout, R.C. Bretherton, J. Decarreau, S. Lee, N. Gregorio, N.I. Edman, M. Ahlrichs, Y. Hsia, D.D. Sahtoe, G. Ueda, A. Sharma, R. Schulman, C.A. DeForest, D. Baker, De novo design of modular protein hydrogels with programmable intra- and extracellular viscoelasticity, Proc. Natl. Acad. Sci. USA 121 (2024), doi:10.1073/pnas.2309457121.
- [25] D.F. Duarte Campos, C.D. Lindsay, J.G. Roth, B.L. LeSavage, A.J. Seymour, B.A. Krajina, R. Ribeiro, P.F. Costa, A. Blaeser, S.C. Heilshorn, Bioprinting cell-and spheroid-laden protein-engineered hydrogels as tissue-on-chip platforms, Front. Bioeng. Biotechnol. 8 (2020) 374, doi:10.3389/fbioe.2020.00374.
- [26] C.Garcia Garcia, S.S. Patkar, B. Wang, R. Abouomar, K.L. Kiick, Recombinant protein-based injectable materials for biomedical applications, Adv. Drug Deliv. Rev. 193 (2022) 114673, doi:10.1016/j.addr.2022.114673.
- [27] A.M. Jonker, D.W.P.M. Löwik, J.C.M. van Hest, Peptide- and protein-based hydrogels, Chem. Mater. 24 (2012) 759–773, doi:10.1021/cm202640w.
- [28] H. Cui, M.J. Webber, S.I. Stupp, Self-assembly of peptide amphiphiles: from molecules to nanostructures to biomaterials, Biopolymers 94 (2010) 1–18, doi:10.1002/bip.21328.
- [29] A.D. Theocharis, S.S. Skandalis, C. Gialeli, N.K. Karamanos, Extracellular matrix structure, Adv. Drug Deliv. Rev. 97 (2016) 4–27, doi:10.1016/j.addr.2015.11.001.
- [30] S. Das, R.S. Jacob, K. Patel, N. Singh, S.K. Maji, Amyloid fibrils: versatile biomaterials for cell adhesion and tissue engineering applications, Biomacromolecules 19 (2018) 1826–1839, doi:10.1021/acs.biomac.8b00279.
- [31] Z. Álvarez, A.N. Kolberg-Edelbrock, I.R. Sasselli, J.A. Ortega, R. Qiu, Z. Syrgiannis, P.A. Mirau, F. Chen, S.M. Chin, S. Weigand, E. Kiskinis, S.I. Stupp, Bioactive scaffolds with enhanced supramolecular motion promote recovery from spinal cord injury, Science 374 (2021) 848–856, doi:10.1126/science.abh3602.
- [32] R. Wang, Z. Wang, Y. Guo, H. Li, Z. Chen, Design of a RADA16-based self-assembling peptide nanofiber scaffold for biomedical applications, J. Biomater. Sci. Polym. Ed. 30 (2019) 713–736, doi:10.1080/09205063.2019.1605868.
- [33] L.D. Koh, Y. Cheng, C.P. Teng, Y.W. Khin, X.J. Loh, S.Y. Tee, M. Low, E. Ye, H.D. Yu, Y.W. Zhang, M.Y. Han, Structures, mechanical properties and applica-

- tions of silk fibroin materials, Prog. Polym. Sci. 46 (2015) 86–110, doi:10.1016/i.progpolymsci.2015.02.001.
- [34] S. Salinas-Fernández, M. Santos, M. Alonso, L. Quintanilla, J.C. Rodríguez-Cabello, Genetically engineered elastin-like recombinamers with sequence-based molecular stabilization as advanced bioinks for 3D bioprinting, Appl. Mater. Today (2019) 100500, doi:10.1016/j.apmt.2019.100500.
- [35] M.J. Webber, J. Tongers, C.J. Newcomb, K.T. Marquardt, J. Bauersachs, D.W. Losordo, S.I. Stupp, Supramolecular nanostructures that mimic VEGF as a strategy for ischemic tissue repair, Proc. Natl. Acad. Sci. USA 108 (2011) 13438– 13443, doi:10.1073/pnas.1016546108.
- [36] A. Froger, J.E. Hall, Transformation of plasmid DNA into E. coli using the heat shock method, J. Vis. Exp. 253 (2007), doi:10.3791/253.
- [37] A. Papadimitropoulos, E. Piccinini, S. Brachat, A. Braccini, D. Wendt, A. Barbero, C. Jacobi, I. Martin, Expansion of human mesenchymal stromal cells from fresh bone marrow in a 3D scaffold-based system under direct perfusion, PLoS ONE 9 (2014) e102359, doi:10.1371/journal.pone.0102359.
- [38] Q. Vallmajo-Martin, N. Broguiere, C. Millan, M. Zenobi-Wong, M. Ehrbar, PEG/HA hybrid hydrogels for biologically and mechanically tailorable bone marrow organoids, Adv. Funct. Mater. 30 (2020) 1910282, doi:10.1002/adfm. 201910282
- [39] K.J. Lampe, A.L. Antaris, S.C. Heilshorn, Design of three-dimensional engineered protein hydrogels for tailored control of neurite growth, Acta Biomater. 9 (2013) 5590–5599, doi:10.1016/j.actbio.2012.10.033.
- [40] S. Zhang, C. Lockshin, A. Herbert, E. Winter, A. Rich, Zuotin, a putative Z-DNA binding protein in Saccharomyces cerevisiae, EMBO J. 11 (1992) 3787–3796, doi:10.1002/j.1460-2075.1992.tb05464.x.
- [41] S. Zhang, T. Holmes, C. Lockshin, A. Rich, Spontaneous assembly of a self-complementary oligopeptide to form a stable macroscopic membrane, Proc. Natl. Acad. Sci. USA 90 (1993) 3334–3338, doi:10.1073/pnas.90.8.3334.
- [42] S. Zhang, T.C. Holmes, C.M. DiPersio, R.O. Hynes, X. Su, A. Rich, Self-complementary oligopeptide matrices support mammalian cell attachment, Biomaterials 16 (1995) 1385–1393, doi:10.1016/0142-9612(95)96874-y.
- [43] F. Gelain, Z. Luo, S. Zhang, Self-assembling peptide EAK16 and RADA16 nanofiber Scaffold hydrogel, Chem. Rev. 120 (2020) 13434–13460, doi:10.1021/ acs.chemrev.0c00690.
- [44] N.L. Goeden-Wood, J.D. Keasling, S.J. Muller, Self-assembly of a designed protein polymer into β -sheet fibrils and responsive gels, Macromolecules 36 (2003) 2932–2938, doi:10.1021/ma025952z.
- [45] B.D. Olsen, J.A. Kornfield, D.A. Tirrell, Yielding behavior in injectable hydrogels from telechelic proteins, Macromolecules 43 (2010) 9094–9099, doi:10.1021/ ma101434a
- [46] C.T.S. Wong Po Foo, J.S. Lee, W. Mulyasasmita, A. Parisi-Amon, S.C. Heilshorn, Two-component protein-engineered physical hydrogels for cell encapsulation, Proc. Natl. Acad. Sci. USA 106 (2009) 22067–22072, doi:10.1073/pnas.0904851106.
- [47] M. van Rosmalen, M. Krom, M. Merkx, Tuning the flexibility of glycine-serine linkers to allow rational design of multidomain proteins, Biochemistry 56 (2017) 6565–6574, doi:10.1021/acs.biochem.7b00902.
- [48] X. Chen, J.L. Zaro, W.C. Shen, Fusion protein linkers: property, design and functionality, Adv. Drug Deliv. Rev. 65 (2013) 1357–1369, doi:10.1016/j.addr.2012.09.
- [49] S. Weisman, V.S. Haritos, J.S. Church, M.G. Huson, S.T. Mudie, A.J.W. Rodgers, G.J. Dumsday, T.D. Sutherland, Honeybee silk: recombinant protein production, assembly and fiber spinning, Biomaterials 31 (2010) 2695–2700, doi:10.1016/j. biomaterials.2009.12.021.
- [50] M. Altman, P. Lee, A. Rich, S. Zhang, Conformational behavior of ionic self-complementary peptides, Protein Sci. 9 (2000) 1095–1105, doi:10.1110/ps.9.6.
- [51] G. Zandomeneghi, M.R.H. Krebs, M.G. McCammon, M. Fändrich, FTIR reveals structural differences between native beta-sheet proteins and amyloid fibrils, Protein Sci. 13 (2004) 3314–3321, doi:10.1110/ps.041024904.
- [52] J.L. Arrondo, A. Muga, J. Castresana, F.M. Goñi, Quantitative studies of the structure of proteins in solution by Fourier-transform infrared spectroscopy, Prog. Biophys. Mol. Biol. 59 (1993) 23–56, doi:10.1016/0079-6107(93)90006-6.
- [53] B. Li, P. Ge, K.A. Murray, P. Sheth, M. Zhang, G. Nair, M.R. Sawaya, W.S. Shin, D.R. Boyer, S. Ye, D.S. Eisenberg, Z.H. Zhou, L. Jiang, Cryo-EM of full-length α-synuclein reveals fibril polymorphs with a common structural kernel, Nat. Commun. 9 (2018) 3609, doi:10.1038/s41467-018-05971-2.
- [54] J. Gao, C. Tang, M.A. Elsawy, A.M. Smith, A.F. Miller, A. Saiani, Controlling selfassembling peptide hydrogel properties through network topology, Biomacromolecules 18 (2017) 826–834, doi:10.1021/acs.biomac.6b01693.
- [55] Y. Cao, S. Bolisetty, J. Adamcik, R. Mezzenga, Elasticity in physically crosslinked amyloid fibril networks, Phys. Rev. Lett. 120 (2018) 158103, doi:10.1103/ PhysRevLett.120.158103.
- [56] J. Schnittert, R. Bansal, G. Storm, J. Prakash, Integrins in wound healing, fibrosis and tumor stroma: high potential targets for therapeutics and drug delivery, Adv. Drug Deliv. Rev. 129 (2018) 37–53, doi:10.1016/j.addr.2018.01.020.

- [57] N. Davidenko, C.F. Schuster, D.V. Bax, R.W. Farndale, S. Hamaia, S.M. Best, R.E. Cameron, Evaluation of cell binding to collagen and gelatin: a study of the effect of 2D and 3D architecture and surface chemistry, J. Mater. Sci. Mater. Med. 27 (2016) 148. doi:10.1007/s10856-016-5763-9.
- [58] V.T. Trossmann, T. Scheibel, Design of recombinant spider silk proteins for cell type specific binding, Adv. Healthc. Mater. 12 (2023) e2202660, doi:10.1002/ adhm.202202660.
- [59] V. Chaturvedi, D.E. Dye, B.F. Kinnear, T.H. van Kuppevelt, M.D. Grounds, D.R. Coombe, Interactions between skeletal muscle myoblasts and their extracellular matrix revealed by a serum free culture system, PLoS ONE 10 (2015) e0127675. doi:10.1371/journal.pone.0127675.
- [60] P.C. Georges, W.J. Miller, D.F. Meaney, E.S. Sawyer, P.A. Janmey, Matrices with compliance comparable to that of brain tissue select neuronal over glial growth in mixed cortical cultures, Biophys. J. 90 (2006) 3012–3018, doi:10. 1529/biophysi.105.073114.
- [61] P. Brun, A. Zamuner, A. Peretti, J. Conti, G.M.L. Messina, G. Marletta, M. Dettin, 3D synthetic peptide-based architectures for the engineering of the enteric nervous system, Sci. Rep. 9 (2019) 5583, doi:10.1038/s41598-019-42071-7.
- [62] V.T. Trossmann, S. Heltmann-Meyer, H. Amouei, H. Wajant, R.E. Horch, D. Steiner, T. Scheibel, Recombinant spider silk bioinks for continuous protein release by encapsulated producer cells, Biomacromolecules 23 (2022) 4427– 4437, doi:10.1021/acs.biomac.2c00971.
- [63] C.Y. Lin, J.C. Liu, Modular protein domains: an engineering approach toward functional biomaterials, Curr. Opin. Biotechnol. 40 (2016) 56–63, doi:10.1016/j. copbio.2016.02.011.
- [64] T. Falcucci, M. Radke, J.K. Sahoo, O. Hasturk, D.L. Kaplan, Multifunctional silk vinyl sulfone-based hydrogel scaffolds for dynamic material-cell interactions, Biomaterials 300 (2023) 122201, doi:10.1016/j.biomaterials.2023.122201.
- [65] M. Dai, J.P. Belaïdi, G. Fleury, E. Garanger, M. Rielland, X. Schultze, S. Lecommandoux, Elastin-like polypeptide-based bioink: a promising alternative for 3D bioprinting, Biomacromolecules 22 (2021) 4956–4966, doi:10.1021/acs.biomac. 1c00861.
- [66] L. Fu, H. Li, Toward quantitative prediction of the mechanical properties of tandem modular elastomeric protein-based hydrogels, Macromolecules 53 (2020) 4704–4710, doi:10.1021/acs.macromol.0c00664.
- [67] L. Li, J.M. Stiadle, E.E. Levendoski, H.K. Lau, S.L. Thibeault, K.L. Kiick, Biocompatibility of injectable resilin-based hydrogels, J. Biomed. Mater. Res. A 106 (2018) 2229–2242, doi:10.1002/jbm.a.36418.
- [68] M. Humenik, M. Magdeburg, T. Scheibel, Influence of repeat numbers on self-assembly rates of repetitive recombinant spider silk proteins, J. Struct. Biol. 186 (2014) 431–437, doi:10.1016/j.jsb.2014.03.010.
- [69] E.T. Pashuck, B.J.R. Duchet, C.S. Hansel, S.A. Maynard, L.W. Chow, M.M. Stevens, Controlled sub-nanometer epitope spacing in a three-dimensional selfassembled peptide hydrogel, ACS Nano 10 (2016) 11096–11104, doi:10.1021/ acsnano.6b05975.
- [70] J.A. Gustafson, R.A. Price, J. Frandsen, C.R. Henak, J. Cappello, H. Ghandehari, Synthesis and characterization of a matrix-metalloproteinase responsive silk-elastinlike protein polymer, Biomacromolecules 14 (2013) 618–625, doi:10.1021/bm3013692.
- [71] V.A. Kumar, N.L. Taylor, S. Shi, B.K. Wang, A.A. Jalan, M.K. Kang, N.C. Wickre-masinghe, J.D. Hartgerink, Highly angiogenic peptide nanofibers, ACS Nano 9 (2015) 860–868, doi:10.1021/nn506544b.
- [72] W. Ye, Z. Yang, F. Cao, H. Li, T. Zhao, H. Zhang, Z. Zhang, S. Yang, J. Zhu, Z. Liu, J. Zheng, H. Liu, G. Ma, Q. Guo, X. Wang, Articular cartilage reconstruction with TGF-β1-simulating self-assembling peptide hydrogel-based composite scaffold, Acta Biomater. 146 (2022) 94–106, doi:10.1016/j.actbio.2022.05.012.
- [73] J.A. Lewis, R. Freeman, J.K. Carrow, T.D. Clemons, L.C. Palmer, S.I. Stupp, Transforming growth factor β-1 binding by peptide amphiphile hydrogels, ACS Biomater. Sci. Eng. 6 (2020) 4551–4560, doi:10.1021/acsbiomaterials.0c00679.
- [74] C. Ligorio, A. Mata, Synthetic extracellular matrices with function-encoding peptides, Nat. Rev. Bioeng. (2023), doi:10.1038/s44222-023-00055-3.
- [75] J. Hwang, K.L. Kiick, M.O. Sullivan, VEGF-encoding, gene-activated collagen-based matrices promote blood vessel formation and improved wound repair, ACS Appl. Mater. Interfaces 15 (2023) 16434–16447, doi:10.1021/acsami. 2c.23022
- [76] S. Zhang, C. Lockshin, R. Cook, A. Rich, Unusually stable beta-sheet formation in an ionic self-complementary oligopeptide, Biopolymers 34 (1994) 663–672, doi:10.1002/bip.360340508.
- [77] Z. Luo, S. Zhang, Designer nanomaterials using chiral self-assembling peptide systems and their emerging benefit for society, Chem. Soc. Rev. 41 (2012) 4736–4754, doi:10.1039/c2cs15360b.
- [78] I. Chiesa, C. Ligorio, A.F. Bonatti, A. De Acutis, A.M. Smith, A. Saiani, G. Vozzi, C. De Maria, Modeling the three-dimensional bioprinting process of β-sheet self-assembling peptide hydrogel scaffolds, Front. Med. Technol. 2 (2020) 571626, doi:10.3389/fmedt.2020.571626.